Chapter 5

Enhancement in properties of PET/clay nanohybrids using 30B nanoclay

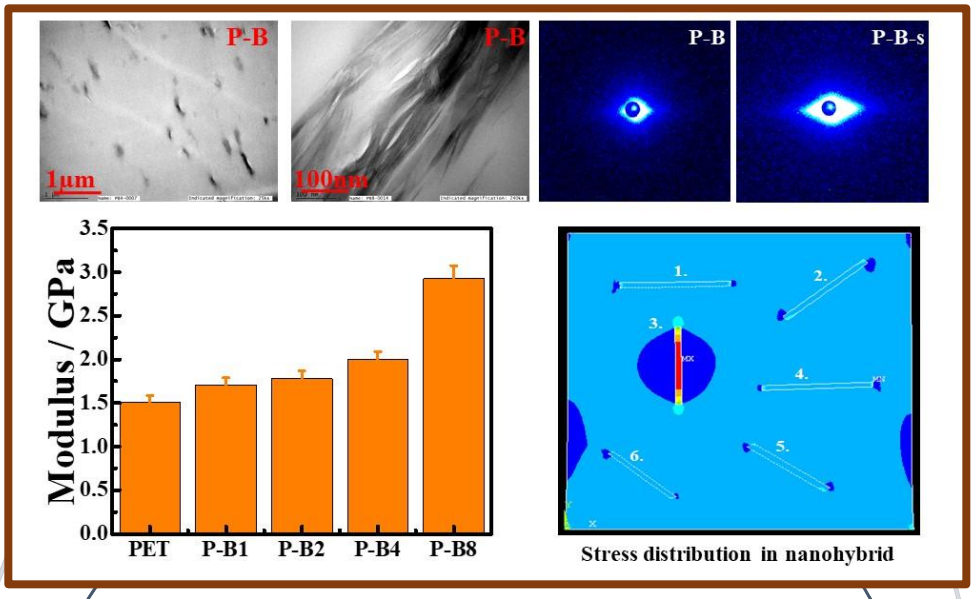

Chapter 5

5.1 Introduction

Cloisite 30B is an organically modified montmorillonite clay which has density of 1.98 g/cc. It is modified using methyl tallow bis-2-hydroxyethyl quaternary ammonium ion exchange. The structure of modifier for Cloisite 30B has been shown in ***Figure 5.1***. Tallow contains mixture of long chain carbons mainly of C_{16} and C_{18}. It has a cation exchange capacity of 100 mequiv. per 100 g. It has lateral dimension of ~250 nm. After it is organically modified, the interplanar distance increases to 1.8 nm from 1.1 nm.

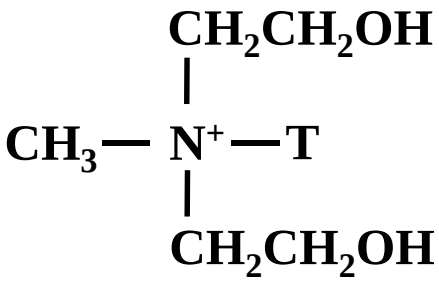

Figure 5.1: *Structure of organic modifier of Cloisite 30B (T is tallow having ~65% C_{18}, ~30% C_{16}, ~5% C_{14})*

Cloisite 15A, Nanolin, layered double hydroxides, fluoromica are the clays which have similar layered structures modified in different ways having different intergallery spacings and cation exchange capacities. Cloisite 30B has previously been used to enhance the properties of nanocomposites [93, 94, 98]. Ghasemi et al. [94] prepared PET/clay nanocomposites prepared through melt casting method and showed meager 20% increment in tensile modulus. The presence of clay induced the increase in modulus, whereas the severe

brittleness was associated with this. Crystallization behavior in the presence of clay was also observed through wide-angle XRD. Scaffaro et al. [91] prepared PET nanocomposites using two different organically modified nanoclays, namely Cloisite 15A and 30B. The melt compounding route was opted to prepare those nanocomposites. Mechanical properties and thermal stability were studied with varying filler concentrations. Young's modulus was not significantly improved until at higher weight percentage of filler concentration (~10 wt%), although the elongation at break dropped drastically even at lower filler content (3 wt%). The thermal stability of the nanocomposites was also reduced as measured through melt rheology and intrinsic viscosity measurements. Ghanbari et al. [98] prepared PET nanocomposites using two organically modified clay (30B and N28E) using melt blending in the presence of multifunctional epoxy-based chain extender. Young's modulus was improved up to 33% using 4 wt% 30B clay, whereas reduction in toughness was around 92%. Yang et al. [96] reported supercritical carbon dioxide pre-dispersed Cloisite 30B melt extruded with PET matrix. The Young's modulus and tensile strength were improved by 12% and ~ 25%, respectively, whereas elongation at break was reduced by ~ 80%. As obvious, there is a need to improve the mechanical strength keeping its toughness intact.

In this work, nanohybrids of PET have been prepared using Cloisite 30B through solution casting route. The dispersion of clay in the PET matrix, clue to generate better mechanical strength, has been studied in detail. The hardness of the nanohybrids has been modeled as measured through Vickers hardness test which, to our best knowledge, has not been worked out previously. The stress distribution in the matrix under tensile loading in presence of nanofillers has been studied. The structural advancement in the nanohybrids has been

examined by SAXS (small-angle X-ray scattering), and the effect of stretching on PET nanohybrids has been studied in detail.

5.2 Experimental

Materials: PET, Cloisite 30B clay (supplied by Southern Clay, U.S.), DCM as solvent.

Preparation of nanohybrid: Nanohybrids of PET and Cloisite 30B clay have been prepared through solvent casting route using Cloisite 30B as filler as explained in ***Chapter 2***. PET nanohybrids have been abbreviated as P-B1, P-B2, P-B4, P-B8 for 1, 2, 4 and 8 percentage of nanoclay concentration respectively. Abbreviation P-B have been used for the 4% of clay concentration.

5.3 Results and discussion

5.3.1 Dispersion and interactions

The prediction about the nanoclay dispersion in PET matrix can be deduced from conclusive TEM and XRD results. The dispersion of nanoclays in polymer matrix has been compared through TEM analysis. The TEM images, shown in ***Figure 5.2a,*** describe the dispersion of the nanoclay in the PET matrix. The 30B clay platelets have been dispersed in the polymer matrix uniformly as can be seen in the low magnification TEM image of ***Figure 5.2a***. The intercalated and some exfoliated morphology can be seen in the high magnification image of ***Figure 5.2a,*** inset image show the increased intergallery spacing due to intercalation of polymer chains between clay platelets. The clay platelets have average aspect ratio (ratio of length and thickness of nanoparticle aggregate) of ~20 and average correlation length (*i.e.* distance between two nanoparticles) [171, 172] of 430 nm.

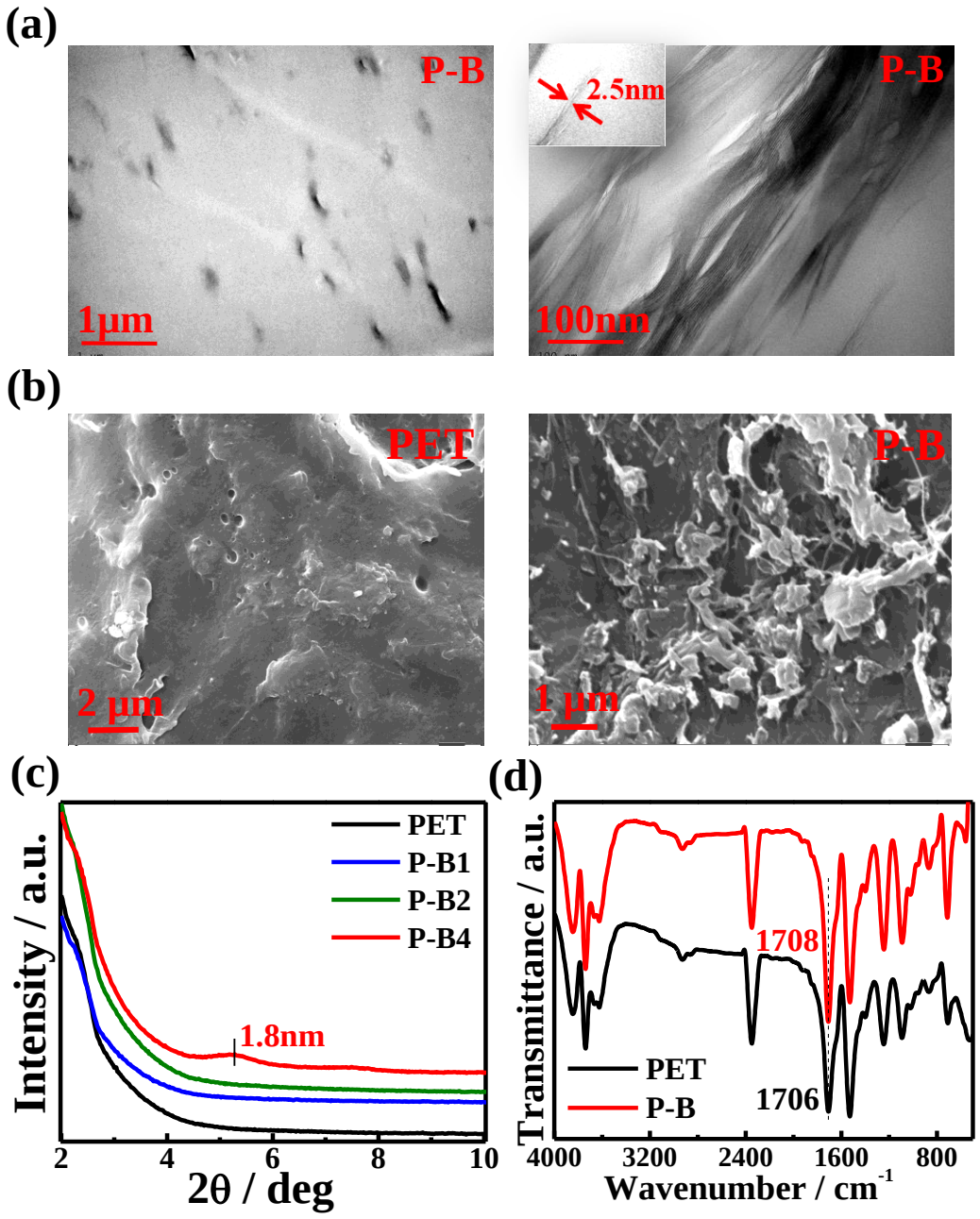

Figure 5.2: ***(a)*** *TEM images of the P-B nanohybrid at low (left) and high magnification (right), inset figure shows the intercalation;* ***(b)*** *SEM images of pure PET and P-B showing the surface morphology;* ***(c)*** *XRD spectra of pure PET and P-B at different nanoclay concentrations; and* ***(d)*** *FTIR spectra showing interactions in nanohybrid.*

Hence, the TEM images show good level of intercalation and some exfoliation of the nanoclay platelets in the PET nanohybrids. The XRD patterns of the nanohybrids have been shown in ***Figure 5.2b***. For the lower percentage of nanoclay inclusion, there is no clear peak to identify d-spacing. The absence of well defined peak could be due to the random orientation / disordered structure of the nanoclay in the polymer matrix. This signifies that there is very less ordering of the clay platelets distribution in the polymer matrix. The peak at 1.8 nm (pure 30B clay has its characteristic peak at 1.8nm) in nanohybrid containing high clay concentration could be due to the fact that the nanohybrids have some unintercalated structure or there is structure formation in the nanohybrid. There exist different kinds of tactoids which are not perfectly ordered and are having different interlayer distances resulting less coherency. However, the clear intercalation can be seen in the TEM images (inset of ***Figure 5.2a***) whereas it is not so evident in XRD spectra presumably because of disordered structure. SEM images of the nanohybrids have been shown in ***Figure 5.2b***. The morphology of nanohybrids shows the presence of nanoclay in PET matrix. The surface roughness has increased in the presence of nanoclay. FTIR spectroscopy has been performed to check the interactions of nanoclay and PET. The carbonyl (C=O) peak has slightly been shifted from 1706 to 1708 cm^{-1} in the nanohybrid [231]. The peak at 709 cm^{-1}, due to ring C-C bending and ring C-H out of plane stretching, has been shifted to 713 cm^{-1} [189]. These shifting of peaks are due to the interactions of clay with polymer matrix.

5.3.2 Thermal properties and stability

Thermal properties of nanohybrids have been shown in ***Figure 5.3***. The TGA thermograms in ***Figure 5.3a*** shows that there is very slight reduction in degradation temperature of P-B nanohybrid (the degradation temperature has been taken at temperature corresponding to 5%

weight loss). The degradation temperature of P-B has come out to be 408 ^{o}C, whereas the degradation temperature of pure PET has been found to be 410 ^{o}C.

The mere fall in degradation temperature is due to the collapse of the clay platelets because of the degradation of the modifier present in the nanoclay gallery at higher temperature during processing the film. This is to mention that the degradation of 30B starts around 182^{o}C [91]. The glass transition temperature has been shown both through DTA and DSC thermograms in ***Figure 5.3a*** (inset) and ***Figure 5.3b***, respectively. The glass transition temperature has been found out to be the same *i.e.* 65 ^{o}C and there is no reduction/increase in glass transition temperature in presence of nanoclay.

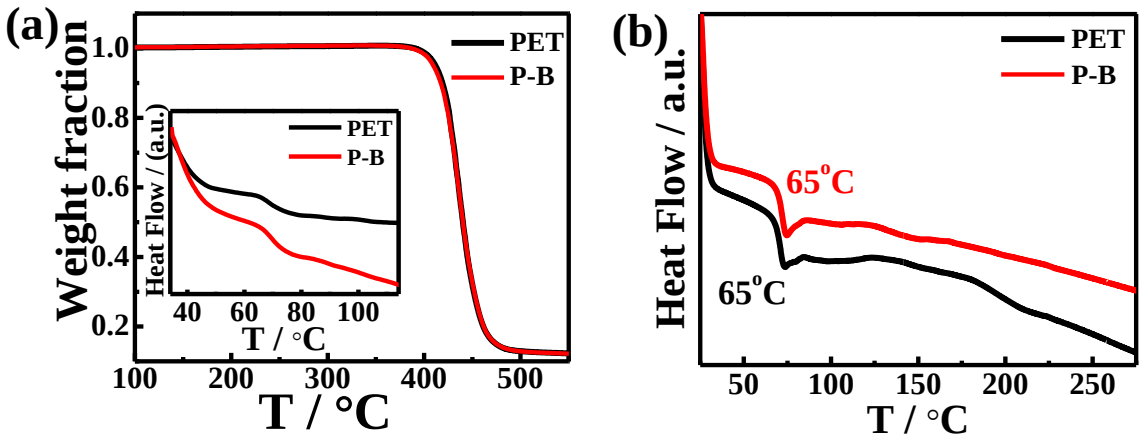

Figure 5.3: (a) *TGA thermograms of pure PET and P-B nanohybrids, inset figure shows the glass transition temperature through DTA thermograms;* ***(b)*** *DSC thermograms showing glass transition temperature of pristine PET and P-B nanohybrid.*

5.3.3 Mechanical responses and predictions

The mechanical properties of the nanohybrids have been shown in ***Figure 5.4***. The stress-strain curves of P-B have been shown in ***Figure 5.5 a***. The modulus of nanohybrids has been shown in ***Figure 5.6 b***. The modulus has been increasing with the increment of the nanoclay content. The toughness is shown in ***Figure 5.7 c***. The 30B clay induces significant increase in Young's modulus (93%) for 8 wt. % of nanoclay inclusion. It can be seen that the toughness of the nanonybrids has been retained up to 4 wt. % of clay concentration. The previous studies have reported huge toughness reductions more than 90% at 4 wt. % of clay loadings [91, 98]. In this study, the toughness reduction is merely 12% for 4 wt. % of filler concentration. However, the increasing amount of 30B is inducing brittleness. The elongation at break is reducing at 8 wt. % of 30B inclusion. The increase of modulus for 8 wt. % nanoclay concentration has been consolidated with the increased brittleness. The increase in brittleness with higher 30B concentration has been reported previously [98]. The toughness in P-B nanohybrids has been reduced for 8 wt. % nanoclay which could be attributed to the agglomeration of the clay particles as well as interfacial debonding which results in voids and flaws in the matrix causing early failure of the material. Although previously reported results showed that the toughness reduced by more than 90% at lower percentage of clay [98]. This sudden decrement at even lower percentage of clay was possible because of melt extrusion process where nanoclay degraded to a greater extent. In this work, solution casting route has been adopted in which the processing temperature has not been that high. Hence, the clay degradation has not been occurred causing considerably high modulus and very low reduction in toughness at 4 wt. % nanoclay (P-B4). The toughness reduction for 4 wt. % of nanoclay inclusion has been mere 12%. The 4 wt. % nanoclay

inclusion has been the optimum where the modulus increment of 21% and toughness reduction only 12% has been achieved. This balance of increment of modulus retaining toughness is better than previously reported studies [91, 94, 98]. The values of modulus for different filler concentrations have been predicted by different micromechanical models.

Prediction of the Young's modulus using micromechanical models

The experimental values have been predicted using the micromechanical model explained in *Chapter 3*. Fitting of these models with the experimental data have been shown in ***Figure 5.4d***. The Halpin Tsai model and Hui-Shia model have predicted the values very closely. Halpin Tsai model predicts the modulus values at different aspect ratios where average value of aspect ratio is taken. Hence, this model gives the close prediction for the elastic modulus. Hui-Shia model predicts the modulus values at an average aspect ratio of 12 whereas the Halpin Tsai fits at an average aspect ratio of 4. The aspect ratio from the TEM images has been calculated as 20. The difference in the aspect ratio for both fitting models and practical value is due to the fact that the formation of both the model is based on different assumptions. Halpin Tsai model takes the random dispersion of the particles but it does not consider the filler particles interaction with the matrix. On the other hand, Hui-Shia model takes the assumption of the unidirectionally oriented particles as well as the perfect interfacial bonding between the filler and the matrix. However, the practical arrangement is very different. The filler particles do not have a constant geometry throughout the composite but instead have random distribution of shapes and sizes. Some filler particles are exfoliated in the matrix whereas most are intercalated. There are particles which get agglomerated also. In all these conditions the aspect ratio gets changed. There are interfacial interactions present between the matrix and filler particles due to which property enhancement is affected to a great extent.

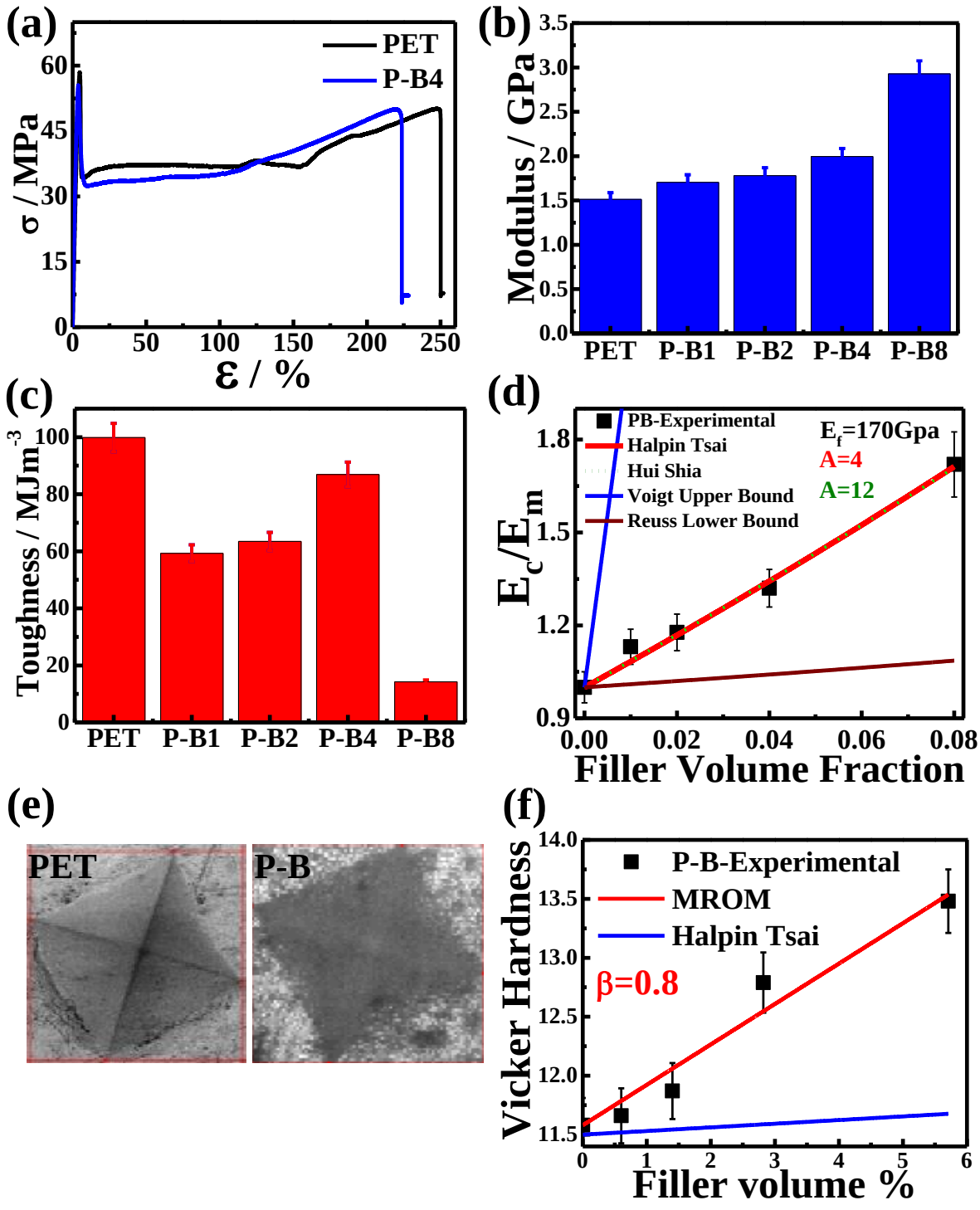

Figure 5.4: ***(a)*** *Stress-strain curves of nanohybrids at different indicated concentrations comparing pure PET;* ***(b)*** *Elastic modulus values of indicated nanohybrids at different filler concentrations as calculated from the stress-strain curve;* ***(c)*** *Toughness values of the*

nanohybrids at different filler concentration as calculated from the area under stress-strain curves; ***(d)*** *Prediction of elastic modulus values using different micromechanical models;* ***(e)*** *Vicker hardness test imprints on the pure PET and P-B nanohybrid; and* ***(f)*** *Prediction of hardness values using different models as discussed in the main text.*

The impurities and the micro voids are also present in the matrix. All of these factors contribute in the alteration of the experimental results and thus are different from what is predicted theoretically. Voigt upper bound [191] and Reuss lower bound [188] models have shown the upper and lower limits of modulus prediction. The experimental values and predicted values are lying between the two limits. However, the improvement in mechanical properties is well predicted through the Halpin-Tsai and Hui Shia models at the aspect ratio values of 4 and 12, respectively. Hence, both the micromechanical models predict the values closely for the systems presented and are suitable for this system.

5.3.4 Microhardness of nanohybrids

The hardness of the samples has been found out through Vickers hardness test. The indentations on pure PET and P-B nanohybrids have been shown in ***Figure 5.4e***. The nanohybrids have clay particles hence showing comparatively darker imprints. The hardness values have been increasing for the increased filler percentage which has been shown in ***Figure 5.4f*** (experimental curve). The clay particles induce stiffness in the polymer matrix which is the reason of the increased hardness of the nanohybrids. The dispersed nanoclay particles form a network structure so that better stress transfer occurs. Moreover, the interactions and interfacial bonding between nanoclay particles and polymer matrix also play a role in increased hardness of the nanohybrids. The hardness is also linearly dependent on

the Young's modulus of the material and as the modulus has been increasing continuously with the filler percentage, the microhardness has also been following the same behavior [235]. In previous reported values, the filler hardness was 83 times the matrix hardness and the increment in nanocomposite hardness is 14% for 7 volume percentage of the filler (Al_2O_3) [195]. Here in this work, the filler hardness is very less *i.e.* 1.28 times the matrix hardness and the hardness increment has been achieved is 16% for 6 volume percentage of the filler. The hardness achievement, in spite of the fact that the filler hardness is not very high, is due to the reason that the filler has large aspect ratio. The clay platelets form structure and induce stiffness in the matrix causing greater hardness. The prediction of the hardness values has been done by the two models named MROM (Modified Rule of Mixtures) [193] and Halpin Tsai model [195].

The values of matrix hardness has been taken as 11.54VHN and nanoclay hardness as 14.88VHN [193]. The MROM predicts the values very closely at a fitting parameter of 0.8. The value of fitting parameter varies proportional to the aspect ratio [236]. Here, the higher value of fitting parameter as compared to previous reported value [195] is due to the higher value of aspect ratio and lower difference in hardness of polymer matrix and filler. Halpin Tsai model under predicts the hardness values. The reason behind this could be the variation in aspect ratio as well as lower difference in hardness values of polymer matrix and filler. Hence, the MROM model is best suited for the prediction of the hardness of the PET nanohybrids at a fitting parameter of 0.8.

5.3.5 Analysis of stress distribution

The distribution of stress in the matrix in presence of nanoparticles has been shown by ANSYS software. The dimensions of the two dimensional polymer plate have been taken as 500×500 nm^2 and the dimensions of dispersed nanoparticles have taken as length ~100nm and thickness of 10nm.

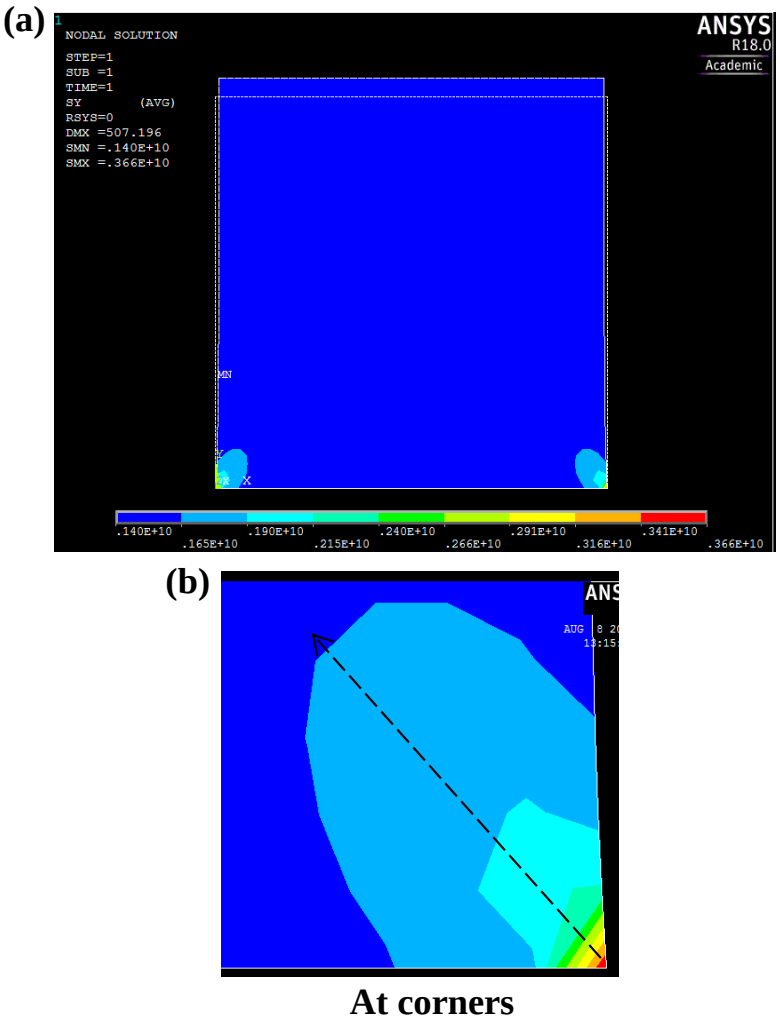

Figure 5.5: *Stress distribution in pure PET matrix (values are indicative not exact);* ***(a)*** *Pure PET matrix under tensile loading in vertical direction;* ***(b)*** *Stress distribution at the corners of the matrix.*

The properties as input are given as: for polymer matrix: Young's modulus = 1.51GPa, Poisson's ratio = 0.33; for nanoparticles: Young's modulus = 170 GPa, Poisson's ratio = 0.23. The nanoparticle and matrix interface are taken as perfectly bonded. The bottom part of the plate has been fixed and tensile force has been applied on the upper part. Pure PET and its nanohybrids' output on applying tensile force has been shown in ***Figure 5.5*** and ***Figure 5.6*** respectively, where the values shown are indicative not exact [237].

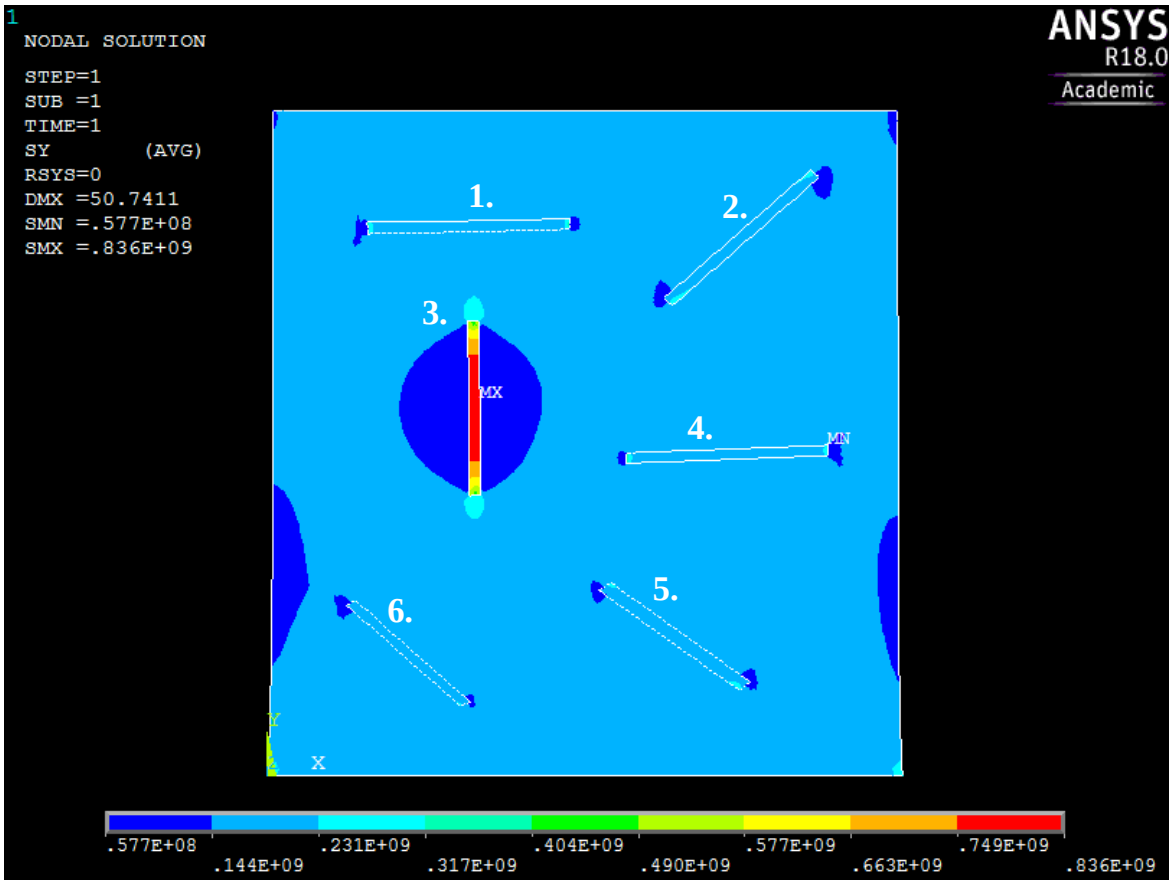

Figure 5.6: *Stress distribution in matrix of PET nanohybrid containing randomly dispersed nanoparticles (values are indicative not exact)*

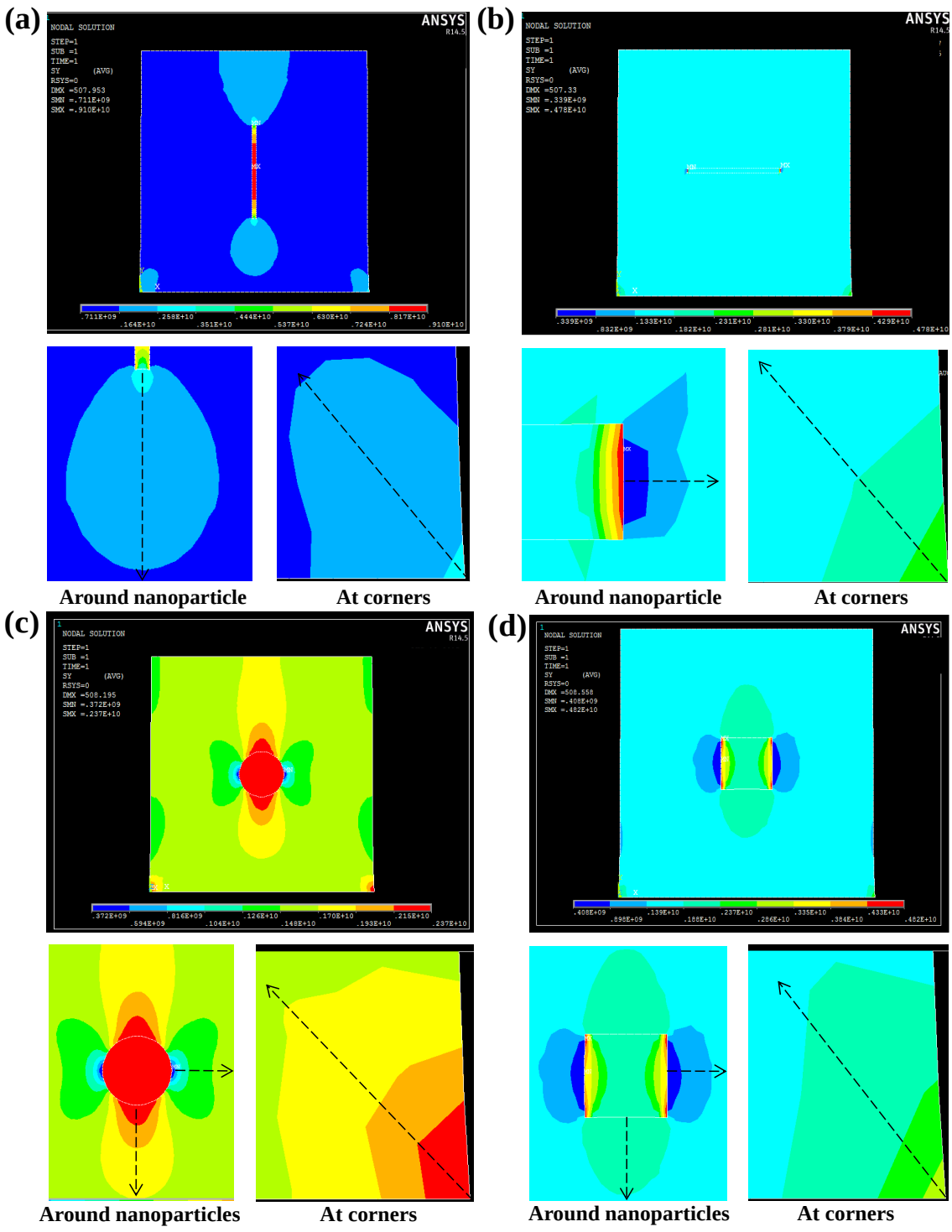

Figure 5.7: *Stress distribution in matrix of PET nanohybrid under tensile loading in vertical direction in presence of* ***(a)*** *Single nanoparticle parallel to the direction of applied load;* ***(b)*** *nanoparticle perpendicular to the direction of the applied load;* ***(c)*** *circular nanoparticle;*

*and **(d)** square nanoparticle (subsequent images show stress distribution in matrix around nanoparticle and at the corner of the matrix as shown by dashed arrow).*

Pure PET has shown the stress distributed uniformly in the matrix (***Figure 5.5a***). The concentrated stress distribution in the corners is due to the fixing of the plate from the bottom (***Figure 5.5b***). The nanohybrid have been shown as the PET matrix containing randomly dispersed nanoparticles at different angles ***Figure 5.6***. When the nanoparticles are randomly dispersed in the matrix and the tensile force is applied, the stress distribution changes. Most of the stress is taken up by the nanoparticles and the stress distributed in the matrix reduces.

The particles aligned perpendicular to the direction of applied load bear the same load as the matrix through their length and have concentrated stress at their ends (***Figure 5.7b)***. The matrix adjacent to it has the minimum stress which gradually increases with increasing length farther from the nanoparticle. The stress at corner of the matrix has been decreased as compared to the stress in pure PET matrix's corners. The circular and square nanoparticle has also been shown in ***Figure 5.7c*** and ***d***. The stress beside the filler particle has been decreased. The nanoparticle bears the maximum stress and the stress in the matrix around the nanoparticle gradually decreases.

Overall, the stress borne by the matrix reduces via nanoparticles embedment. The particles aligned in the direction of applied load bear the maximum stress as can be seen in ***Figure 5.6***. In presence of the nanoparticles, the polymer matrix bears the lesser amount of the stress as compared to the pure polymer matrix. This conclusion is dependent on the various factors with the most prime factor being the interfacial interactions along with the homogeneous dispersion of nanofillers, presence of impurities, agglomerations etc. Here, the stress

distribution was observed with the assumptions of perfect interfacial bonding and absence of impurities.

5.3.6 Effect of stretching on structure

The effect of stretching has been observed through SAXS and wide angle XRD studies. The SAXS images of unstretched and stretched samples have been shown in ***Figure 5.8a***. The unstretched samples have shown a uniform ring because of the uniform distribution of the nanoclay in the nanohybrid. Upon stretching the samples, the SAXS patterns have shown a streak occurring perpendicular to the stretching direction. This is the result of the partial orientation of clay particles and short range ordering in the polymer matrix. The streak can also be the result of the elongation of voids present in the matrix [205]. Intensity ($I(q)$) vs scattering vector (q) has been plotted in ***Figure 5.8b***. The peak appears at 39nm which is more evident in the Lorentz corrected profile ($I(q).q^2$ vs q plot) in ***Figure 5.8c***. The peak shows the characteristic length of 37 nm in unstretched P-B which has been increased to 39 nm in the stretched nanohybrid. The increase in the characteristic peak is due to the short range ordering and the partial alignment of the clay particles in the stretching direction. The correlation lengths of the blob (determined by Debye Bueche model [173, 207]) have found to be increasing upon stretching the sample (***Figure 5.8d***). The blob size is further increasing in presence of nanoclay. WAXD pattern of the unstretched and stretched samples have been shown in ***Figure 5.8e***.

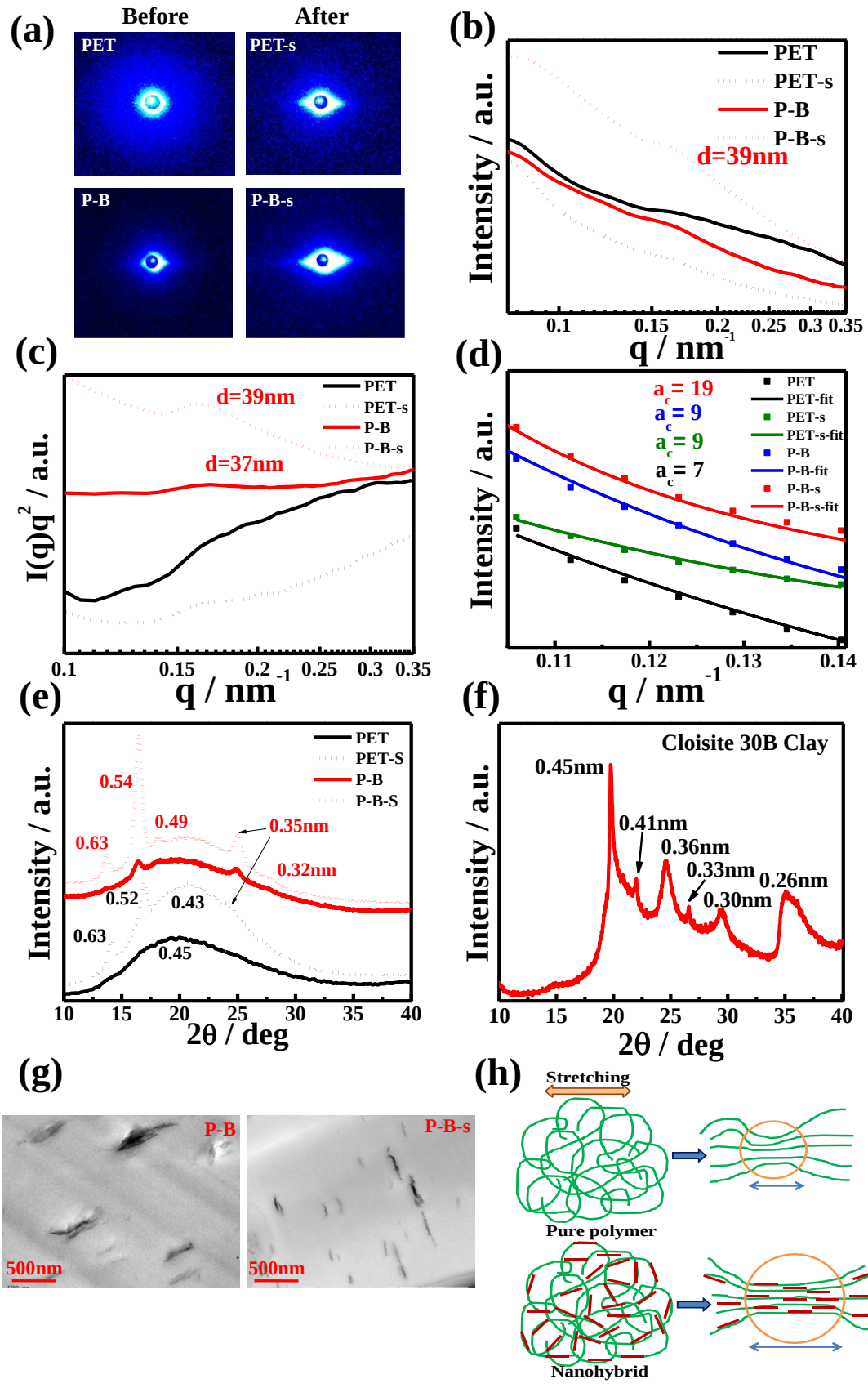
(a)
Before
After
PET
PET-s
P-B
P-B-s
(b)
PET
PET-s
P-B
P-B-s
d=39nm
Intensity / a.u.
q / nm-1
(c)
d=39nm
d=37nm
PET
PET-s
P-B
P-B-s
I(q)q2 / a.u.
q / nm-1
(d)
ac = 19
ac = 9
ac = 9
ac = 7
PET
PET-fit
PET-s
PET-s-fit
P-B
P-B-fit
P-B-s
P-B-s-fit
Intensity / a.u.
q / nm-1
(e)
PET
PET-S
P-B
P-B-S
0.54
0.49
0.35nm
0.63
0.32nm
0.52
0.43
0.63
0.45
Intensity / a.u.
2θ / deg
(f)
Cloisite 30B Clay
0.45nm
0.41nm
0.36nm
0.33nm
0.26nm
0.30nm
Intensity / a.u.
2θ / deg
(g)
P-B
500nm
P-B-s
500nm
(h)
Stretching
Pure polymer
Nanohybrid

Figure 5.8: ***(a)*** *SAXS images of unstretched and stretched samples of PET and P-B,* ***(b)*** *Intensity vs. wavevector plot extracted from the SAXS images;* ***(c)*** *Lorentz corrected profiles of the unstretched and stretched samples;* ***(d)*** *Debye Bueche model fitting for calculation of correlation lengths of unstretched and stretched samples;* ***(e)*** *Wide angle XRD plots of unstretched and stretched samples;* ***(f)*** *Wide angle XRD plots of pure Cloisite 30B clay;* ***(g)*** *High magnification TEM images of unstretched and stretched P-B nanohybrid; and* ***(h)*** *Schematic diagram of the structural advancement upon stretching in PET and P-B nanohybrids.*

The unstretched sample of PET has shown a hump having peak at 0.45 nm which signifies the amorphous structure of the polymer matrix (texturing). WAXD pattern of unstretched P-B have shown some characteristic peaks of 30B nanoclay at 0.54 and 0.35nm. WAXD spectra of 30B clay has been given in ***Figure 5.8f***. On stretching the nanohybrid, the intensities of the characteristic peaks have increased and few more characteristic peaks have also appeared (0.49 and 0.32 nm). The increased intensity is due to the induced coherency in the molecular structure because of the presence of nanoclay. The average aspect ratio of the nanoclay particles have also been increased from 20 to 47 on stretching as can be seen from ***Figure 5.8g***.

The nanoclay particles tend to align the molecular chains more and hence increase the blob size. The clay platelets between the polymeric chains align themselves as well as the polymeric chains. The effect of stretching on the molecular structure has been shown in the schematic ***Figure 5.8h*** where blob size has been shown increasing on stretching the nanohybrid. However, the mechanical strength has improved in PET nanohybrid significantly without any considerable loss of toughness as compared to literature reports. The dispersion of nanoclay and nanostructural arrangement under uniaxial stretching is

responsible for those properties development as opposed to degradation in melt processed nanohybrid.

5.4 Conclusion

PET nanohybrids have been prepared through solvent casting route. The dispersion of nanoclay have been tested through TEM and XRD and found to be homogeneous and uniform. The interactions of nanoclay with PET matrix have been observed using FTIR. Thermal properties of nanohybrids have been tested by TGA and DSC where the degradation temperature and glass transition temperature has found to be unchanged. The nanohybrids have shown significant increment in tensile properties and the modulus has been increased up to 93% for 8 wt. % filler concentration. Toughness has been slightly compromised as opposed to huge loss in literature reports. The optimum value for the modulus and toughness has been obtained at 4% filler concentration where modulus has been increased 21% and toughness reduction has been 12% only. Hardness of the nanohybrids has been tested by Vickers hardness test where the hardness has increased up to 16% for 8 wt. % of filler concentration in nanohybrid. The analysis of stress distribution in presence of nanoclay has been done using ANSYS software. The clay particles have been found to bear most of the stress in nanohybrids. Effect of stretching on the structure has been studied using SAXS of pure PET and PET nanohybrid. The presence of clay in the polymer matrix has increased the local structuring/ordering which has also been reflected in the wide angle XRD patterns. The method proposed results in retaining toughness which is important for the material to be used in various applications. The effect of geometry of fillers on the stress distribution has been studied so as to impart the light on the behavior of nanofillers in different orientation. The stretching behaviors of nanohybrids have been studied to observe the effect of nanoclay in

PET matrix. The PET nanohybrids have been found to have practical usage due to improved properties.